

Non-Hermitian magnon-photon interference in an atomic ensemble

Rong Wen,¹ Chang-Ling Zou,⁵ Xinyu Zhu,¹ Peng Chen,¹ Z. Y. Ou,⁴ J. F. Chen,^{1,3,†} and Weiping Zhang^{2,3,†}

¹*Quantum Institute for Light and Atoms, Department of Physics,
East China Normal University, Shanghai 200241, China*

²*Department of Physics and Astronomy, Shanghai Jiao Tong University, Shanghai 200240, China*

³*Collaborative Innovation Center of Extreme Optics,
Shanxi University, Taiyuan, Shanxi 030006, China*

⁴*Department of Physics, Indiana University-Purdue University Indianapolis,
402 North Blackford Street, Indianapolis, Indiana 46202, USA*

⁵*Key Laboratory of Quantum Information, University of Science and Technology of China, Hefei, 230026, China*

[†]*e-mail: jfchen@phy.ecnu.edu.cn; wpzhang@phy.ecnu.edu.cn*

(Dated: November 2, 2018)

The beam-splitter (BS) is one of the most common and important components in modern optics, and lossless BS which features unitary transformation induces Hermitian evolution of light. However, the practical BS based on the conversion between different degree of freedoms are naturally non-Hermitian, as a result of essentially open quantum dynamics. In this work, we experimentally demonstrate a non-Hermitian BS for the interference between traveling photonic and localized magnonic modes. The non-Hermitian magnon-photon BS is achieved by the coherent and incoherent interaction mediated by the excited levels of atoms, which is reconfigurable by adjusting the detuning of excitation. Unconventional correlated interference pattern is observed at the photon and magnon output ports. Our work is potential for extending to single-quantum level to realize interference between a single photon and magnon, which provides an efficient and simple platform for future tests of non-Hermitian quantum physics.

An optical linear beam-splitter mixes the photons in different paths to interfere, and it is an essential device in various optical applications, such as the gravitational wave detection [1] and optical coherence tomography [2]. A BS can also manipulate photonic quantum state encoded in different modes, which is the most basic device for building quantum communication network [3–6]. Such a concept in photonics have also been generalized to other excitations, including the phonon [7], plasmon [8], magnon [9], and matter waves [10]. However, almost all of previous studies assume the Hermitian interactions in a closed quantum system. Considerable works demonstrate that it is possible to change the phase factor of the reflection and the transmission coefficients when considering losses in a BS [11], and the quantum operations on photons would be affected by such non-Hermitian system [12]. Until recently, the unconventional coalescence have been demonstrated for interfering single plasmons in a non-unitary BS system [13].

While the non-Hermitian interference is of great importance conceptually and fundamentally, realizing a full controllable non-Hermitian BS is still a challenge. It is anticipated that any conversion process between excitations could be treated as a BS [14, 15], therefore a hybrid atom-light interface provides an appealing and versatile platform to study the photon-matter interference [16, 17]. Driven by an external optical field, magnon in an atomic ensemble, also known as collective atomic spin-wave excitation [18], could be converted to photon. Such an magnon-photon beam-splitter (MPBS) have been extensively studied for quantum storage applications [19, 20] and also are significant media for en-

tangling distant quantum node through light [21].

In this Letter, we realized a non-Hermitian MPBS mixing photons and magnons in cold atomic ensembles. By an ensemble of three-level atoms with near-resonant control laser, reconfigurable coherent and incoherent conversion between traveling photonic and localized magnonic modes is demonstrated. By a temporal Mach—Zehnder interferometer, the interference based on such MPBS have been demonstrated, and the interesting unconventional phenomena of non-Hermitian interference are revealed. Our study provides an versatile experimental platform to study the non-Hermitian physics and parity-time symmetry at single quanta level [22, 23]. By exploiting the multiple level atoms and optical control, our results can be generalized to multiple magnon mode and photons with different color, and even bilinear-form of interactions to study the interplay between gain and loss [24].

As sketched in Fig. 1(a), a cigar-shaped laser cooled ⁸⁵Rb atoms cloud is prepared in a two-dimensional magneto-optical trap (MOT) [25, 26], and the non-Hermitian MPBS is realized by external control laser stimulating conversion between the signal photon and magnon. The underlying quantum processes is explained by the energy level diagram (inset of Fig. 1(a)): a strong control laser (Ω_c) induces coherent conversion between $|2\rangle$ and $|3\rangle$, and also initialize the atom ensemble in the ground state $|1\rangle$; signal photons (Ω_p) can be converted to magnon, i.e. the excitation on level $|2\rangle$, through the intermediate excited state. Due to the spontaneous emission of atomic excited state, there are two incoherent processes associate with the MPBS operation: (i) direct exciting

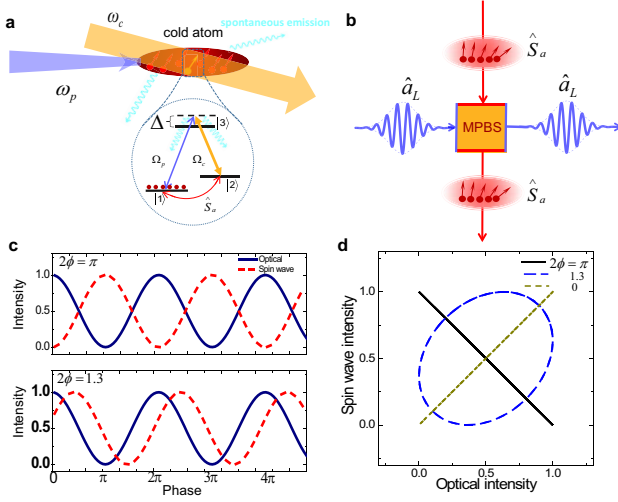


FIG. 1. **Schematics of the non-Hermitian MPBS.** (a) photon-magnon conversion in a three-level atom, where a control beam can stimulate the coherent conversion between the input probe photons and collective atomic excitation between the two metastable states $|1\rangle$ and $|2\rangle$ (magnon), while the spontaneous emission induces an incoherent conversion between photon and magnon. The inset: three-level Λ atomic energy level. Ground state $|1\rangle$ ($|2\rangle$): $5S_{1/2}, F = 2$ ($F = 3$); Excited state $|3\rangle$: $5P_{1/2}, F = 3$. The probe beam and control beam are two-photon resonant. (b) The cold atom ensemble serves as a beam-splitter, where the input optical wave and spin wave interfere. (c) The sinusoidal fringes of interference between the optical wave and spin wave. (d) The phase diagram for the photon and magnon output, with the black solid and green dot lines presenting the phase difference of fringe $2\phi = \pi$ and 0 , respectively. The ellipse represents an arbitrary non-Hermitian beam-splitter.

atoms to the excited state, the signal photon be absorbed and scattered to free space; (ii) the population on $|2\rangle$ be further excited to excited state by the control laser, and decay to $|1\rangle$ by emitting a photon into free space. Although the two decoherence processes would lead to the loss of photon and magnon separately, they are not independent because both processes rely on the same excited state and free-space optical modes. Therefore, the two decoherence processes would interfere on the shared decay channel, allows a indirect magnon-photon conversion process mediated by the decay channels. As a result, the spontaneous emission of excited state contributes an effective incoherent interaction between magnon and photon, which laid as the foundation of the non-Hermitian MPBS studied in this work.

Fig. 1(b) conceptually illustrates the MPBS: a traveling signal photon pulse mode (\hat{a}_L) and a localized magnon mode (\hat{S}_a) are mixed via the MPBS. By preparing input photon and magnons with different initial phase, and interfere them on the MPBS, the intensity of output photon and magnon would show sinusoidal fringes. In Fig. 1(c), the results for a ideal Hermitian

MPBS is plotted, where fringes for photon and magnon show complementary oscillations due to the energy conservation. For a general MPBS, we can introduce a phase factor ϕ for the reflection coefficients ($|r|e^{i\phi}$, $|r'|e^{i\phi}$), with transmission coefficient be real. Therefore, $2\phi = \pi$ for unitary MPBS, and be other values for non-Hermitian MPBS [27]. By plotting the Lissajous curve of the outputs from two-port (Fig. 1(d)), it is found that the non-Hermitian MPBS can change the outputs from anti-correlated ($2\phi = \pi$) to correlated ($\phi = 0$).

The photon-magnon interference in non-Hermitian MPBS is performed by the experimental setup shown in Fig. 2(a). The schematics of the temporal inteferometric setup is shown in Fig. 2(b). It is worth noting that the magnon port is virtual because we do not directly access the magnon, therefore our MPBS is used for interference in time-domain instead of spatial, and the MPBS is implemented three times for magnon state preparation, interference and magnon state readout, respectively. To prepare the magnon, a weak probe pulse is sent to the atomic cloud and converted to the collective ground state spin excitation, which is equivalent to a quantum storage process [28]. To realize the interference by the MPBS, another probe pulse is sent into the atom after the magnon preparation. The MPBS is enabled by the control laser, and the output for the photon is directly collected by a photomultiplier tube (PMT). The output of the magnons are indirectly measured by converted them to photons using another control laser pulse, and such a magnon readout process that depletes the magnon excitation in atomic cloud also serves as an initialization process for next experiment cycle.

Figs 2(d)-(e) show the outputs of the MPBS for the case of single photon detuning 30 MHz with an optical depth (OD) of 30 as an example. In the following experiments, we adjusted the coupling pulse intensities for the magnon preparation and interference steps to match the amplitudes of output photon and magnon [29]. Figure 2(d) shows the results for single port input to MPBS (either photon or magnon be vacuum state), and Fig. 2(e) demonstrates the interference results captured at different relative phase of between the two arms of inteferometer. The output intensities of photon ($n_a = \langle \hat{a}_L^\dagger \hat{a}_L \rangle$) and magnon ($n_s = \langle \hat{S}_a^\dagger \hat{S}_a \rangle$) can hence be obtained by integrating the areas of the output pulses (grey region and the rosiness region) in the Fig. 2(e).

For a simplified model of our experiments based on single magnon mode, the MPBS operation can be described the effective Hamiltonian ($\hbar = 1$) [30]

$$H_{\text{eff}} = \frac{g^2 N}{\Delta - i\kappa_{13}} \hat{a}_L^\dagger \hat{a}_L + \frac{\Omega_c^2}{\Delta - i\kappa_{13}} \hat{S}_a^\dagger \hat{S}_a + \frac{g\sqrt{N}\Omega_c}{\Delta - i\kappa_{13}} \left(\hat{a}_L \hat{S}_a^\dagger - \hat{a}_L^\dagger \hat{S}_a \right) \quad (1)$$

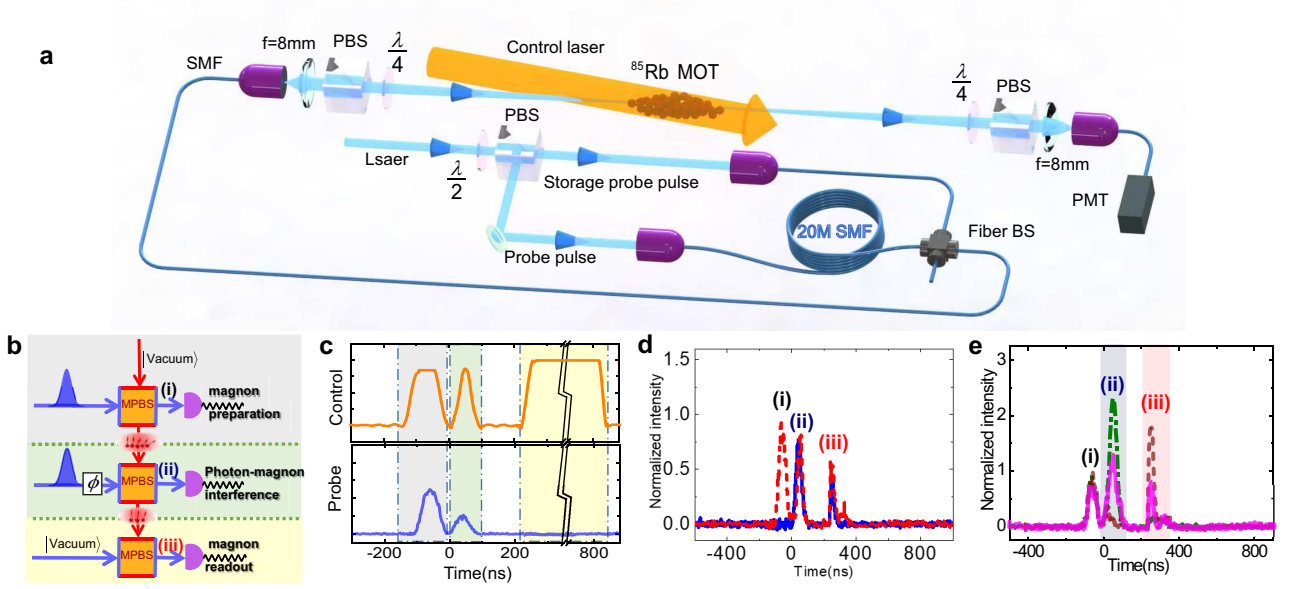


FIG. 2. **Experimental setup.** (a) The weak probe pulse splitting into two pulse are launched into an ^{85}Rb MOT (with 20-meter-fiber inserted) along the longitudinal axis of the atomic cloud, the angle between the control beam and the atom long axis direction is 2.5° . the output for the photon is directly collected by a photomultiplier tube (PMT). (b) Schematic diagram of the Photon-magnon interference. (c) The timing sequence of the control light and the probe light represented by the orange and the blue line. (d) Single port input to MPBS (either photon or magnon be vacuum state) with balanced splitting ratio represented by the blue solid line and the red dash line respectively. (e) photon-magnon interference at different interferometric phase (show 3 results in the figure) when both the optical and spin wave exist.

under the approximations of $|\Delta|^2 + \kappa_{13}^2 \gg g, \Omega_c$ (See SM for more careful treatments). Here, $\Delta = \omega_3 - \omega_1 - \omega_p$ is the detuning, κ_{13} represents the dephasing rate between $|3\rangle$ and $|1\rangle$, g is the atom-photon coupling strength, N is the number of atoms, and Ω_c is the Rabi frequency of the control field. In all experiments, the signal and control light satisfies the two-photon resonance condition, i.e., $\omega_p - \omega_c = \omega_2 - \omega_1$. The last term of Eq. (1) denotes the linear beam-splitter-type of interaction [30], but with a complex coupling strength when we adiabatically eliminate the excited state. The non-zero imaginary part leads to the non-Hermitian [23] photon-magnon conversion in the cold atom ensemble. By considering a square signal photon pulse with duration of τ_p , the spatial-temporal input-output function of the non-Hermitian MPBS reads

$$\begin{pmatrix} S(\tau_p) \\ a(L) \end{pmatrix} = \begin{pmatrix} t & r \\ r' & t' \end{pmatrix} \begin{pmatrix} S(0) \\ a(0) \end{pmatrix}, \quad (2)$$

with the transfer matrix elements $t = e^{-\frac{\zeta}{i\Delta/\kappa_{13}+1}}$, $t' = 1 - \frac{\eta}{\zeta}(1-t)$, $r = t-1$ and $r' = \frac{\eta}{\zeta}r$. Here, $\zeta = \Omega^2\tau_p/\kappa_{13}$ is a dimensionless number quantify the beam-splitter interaction strength and η is a parameter depends on the OD.

From the transfer matrix, the parameter Δ/κ_{13} plays an important role to control the coalescence of MPBS. With far-detuned control, i.e., $\Delta/\kappa_{13} \gg 1$, $T_{11} \approx 1 + i\zeta\kappa_{13}/\Delta$, $T_{22} \approx 1 + i\eta\kappa_{13}/\Delta$, $T_{12} \approx i\zeta\kappa_{13}/\Delta$ and

$T_{21} \approx i\eta\kappa_{13}/\Delta$, the MPBS therefore behaves as a normal lossless BS with $\phi \approx \pi/2$. The phase difference of the interference fringe is π , as shown in Fig. 3(a) and (b). The output intensities at optical wave reaches the maximum while the atomic spin port reaches the minimum value, and vice versa, showing anti-correlation that conserves the number of excitations. Oppositely, near-resonance excitation $\Delta/\kappa_{13} \rightarrow 0$, the MPBS is a lossy BS with off-diagonal terms of T are negative numbers. The outputs are correlated that tends to simultaneously reach extreme values, and the phase difference of fringes is zero, as shown in Fig. 3(c) and (d). An implication of this result is it is in the PT-symmetry broken regime of the non-Hermitian system [12, 23]. There is only one eigenstate as a superposition of photon and magnon, so the ratio n_a/n_s is a constant. For general $0 < 2\phi < \pi$, the $\{n_a, n_s\}$ show a ellipse trajectory.

As indicated by the Eq. (2), the phase difference of interference fringes 2ϕ can be adjusted by controlling the experiment parameters of the MPBS, including the detuning Δ , OD and coupling power (Ω_c). In Fig. 4, we performed more detailed experimentally studied the phase of MPBS by reconstructing the Lissajous curve. In Fig. 4(a1)-(a3), we decrease single photon detuning $\Delta/2\pi$ from 30 MHz to 0 while maintaining OD=40. The experimental data are fitted with blue solid ellipses, which turn into near-circular and change its direction from anti-correlation to correlation with Δ/κ_{13}

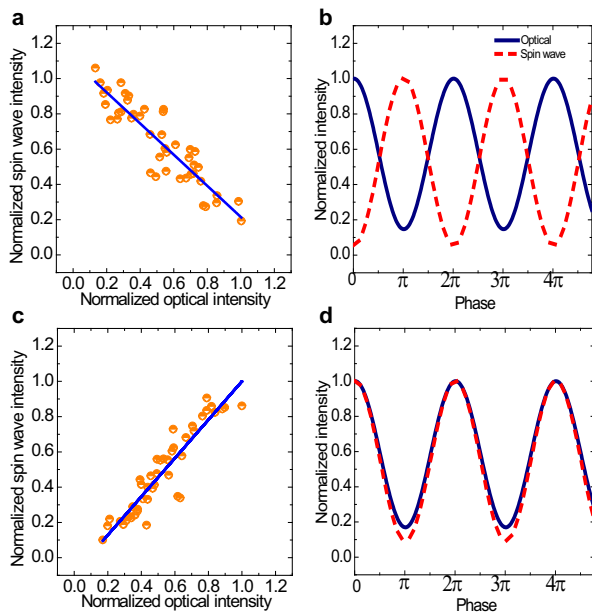


FIG. 3. **The results of the pure Hermitian and non-Hermitian MPBS.** The orange circles represents the smoothed experiments data, with blue solid lines showing the fit correlation and anti-correlation. The sine curve are theory fit experiment data corresponding interference fringe. The navy solid lines represents the optical mode interference fringes, and the red dash lines denote the atomic spin mode. (a)(b) Pure coherent condition, while $OD=40$ and single photon detuning is $\Delta/2\pi = 60$ MHz. (c)(d) non-Hermitian MPBS condition, with $\Delta = 0$ and $OD=40$.

decreases. As summarized in Fig. 4(a4), with theoretical lines calculated from full magnon-photon coupling model [see Supplementary Materials]. Single mode approximation satisfactorily describe the transition from Hermitian to Non-Hermitian. Fig. 4(b1)-(b3) represent the measured phase diagram for different ODs, with fixed $\Delta/2\pi = 30$ MHz, and they are summarized in Fig. 4(b4). For increasing OD, the number of atoms $N \propto OD$ increases, where the single mode approximation breaks down [see Supplementary Materials]. It is can be intuitively understand that a MPBS with increased OD can be treated as a sequence of spatially cascaded single magnon mode-based MPBS, thus the non-Hermitian induced phase would increase with the OD. From Fig. 4(b4), it is clearly demonstrated that the MPBS deviated from Hermitian, i.e. 2ϕ decreases from π , for growing OD. Thus, our MPBS can be easily reconfigured from a nearly-ideal Hermitian model to a non-Hermitian beam-splitter by only changing the laser frequencies or the condition of MOT, would be a convenient platform for future studies of non-Hermitian physics.

In conclusion, we demonstrate a tunable non-Hermitian MPBS in a three-level Λ atomic system driven by a strong coupling field. Through changing the opti-

cal depth and the single photon detuning Δ , we can adjust its non-Hermiticity. The non-Hermitian feature can be observed through interference between optical field and collective atomic spin wave in an equivalent MZ-interferometer setup. The phase difference of the interference fringes between the optical mode and the atomic spin mode can be adjusted from π , complementary to 0, correlated. A direct implication is the bosons change their coalescence through this MPBS. This is caused by the non-unitary transformation induced by incoherent photon-magnon interaction. Finally, our work can extend to single-quantum level to realize Hong-Ou-Mandel interference between a single photon and a single atomic spin mode. The non-Hermitian atomic beam-splitter lay the foundation for verify P-T symmetry in three-level EIT system, and how the quantum statistics of bosons and fermions change in such exotic system.

-
- [1] The LIGO Scientific Collaboration, Observation of Gravitation Waves from a Binary Black Hole Merger. *Phys. Rev. Lett.* **116**, 061102 (2016).
 - [2] Lvovsky, A. I., Raymer M. G. Continuous-variable optical quantum-state tomography. *Rev. Mod. Phys.* **81**, 299-332 (2009).
 - [3] Hariharan, P. Optical interferometry. *Rep. Prog. Phys.* **54**, 339-390 (1991).
 - [4] Zukowski, M., Zeilinger, A., Horne, M. A. & Ekert, A. K. 'Event-ready-detectors' Bell experiment via entanglement swapping. *Phys. Rev. Lett.* **71**, 4287-4290 (1993).
 - [5] Walther, P. *et al.* De Broglie wavelength of a non-local four-photon state. *Nature* **429**, 158-161 (2004).
 - [6] Lenef, A. *et al.* Rotation Sensing with an Atom Interferometer. *Phys. Rev. Lett.* **78**, 760-763 (1997).
 - [7] Toyoda, K. Hiji, R. Noguchi, A. & Urabe, S. Hong-Ou-Mandel interference of two photons in trapped ions. *Nature* **527**, 74-77 (2015).
 - [8] Fakonas, J. S., Lee, H., Kelaita, Y. A. & Atwater, H. A. Two-plasmon quantum interference. *Nat. Photonics* **8**, 317-320 (2014).
 - [9] A. V. Chumak, V. I. Vasyuchka, A. A. S. & B.H. Magnon spintronics. *Nat. Phys.* **11**, 453-461 (2015).
 - [10] Lopes, R. *et al.* Atomic Hong-Ou-Mandel experiment. *Nature* **520**, 66-68 (2015).
 - [11] Barnett, S. M., Jeffers, J., Gatti, A. & Loudon, R. Quantum optics of lossy beam splitters. *Phys. Rev. A* **57**, 2134-2145 (1998).
 - [12] Li. M. *et al.* Effect of unbalanced and common losses in quantum photonic integrated circuits. *Chinese Opt. Lett.* **15**, 092701 (2017).
 - [13] Vest, B. *et al.* Anti-coalescence of bosons on a lossy beam splitter. *Science* **356**, 1373-1376 (2017).
 - [14] Ou, Z. Y. Efficient conversion between photons and between photon and atom by stimulated emission. *Phys. Rev. A* **78**, 023819 (2008).
 - [15] Reim, K. F. *et al.* Multipulse addressing of a Raman quantum memory: configurable beam splitting and efficient readout. *Phys. Rev. Letts.* **108**, 263602 (2012).
 - [16] Qiu, C. *et al.* Atom - light superposition oscillation and

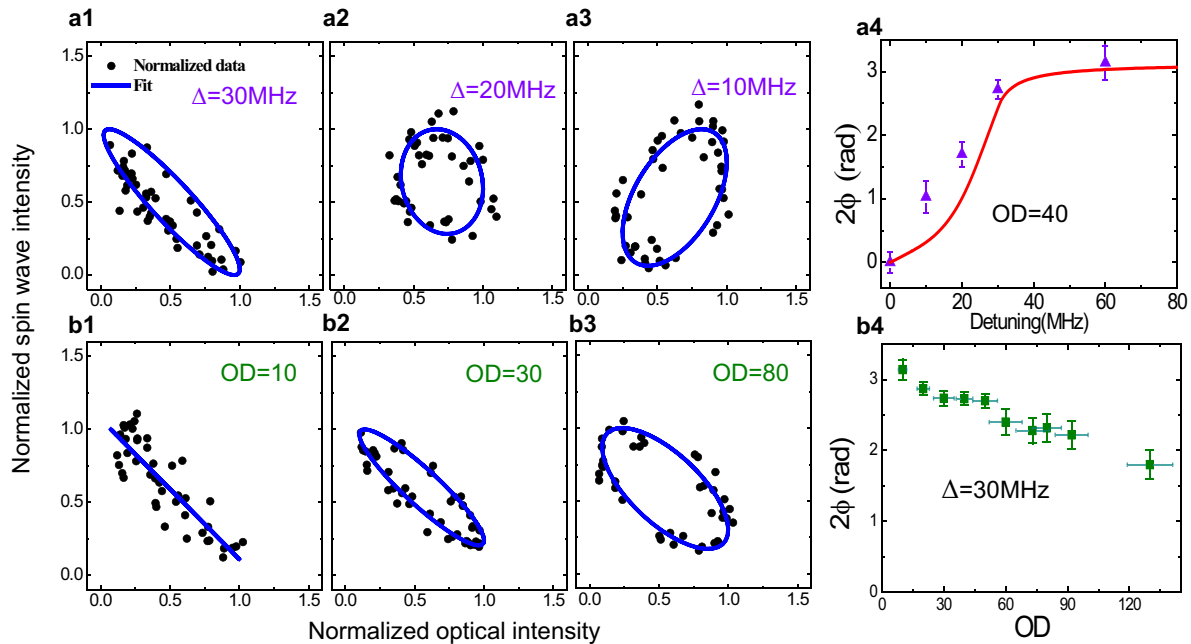


FIG. 4. **The phase diagram for different experiment parameter of photon-magnon interference.** The black dots represents the experiments data, and the blue solid lines shows theory fit curve. The experiments data were plotted through normalization processing. (a1)-(a4) OD= 40 with different single photon detuning Δ . (b1)-(b4) Single photon detuning $\Delta/2\pi = 30$ MHz with different OD.

Ramsey-like atom - light interferometer. *Optica* **3**, 775-780 (2016).

- [17] Campbell, G., Hosseini, M., Sparkes, B. M., Lam, P. K. & Buchler, B. C. Time- and frequency-domain polariton interference. *New J. Phys.* **14**, 033022 (2012).
- [18] Fleischhauer, M. & Lukin, M. D. Dark-state polaritons in electromagnetically induced transparency. *Phys. Rev. Lett.* **84**, 5094-5097 (2000).
- [19] D. F. Phillips, A. Fleischhauer, A. Mair, R. L. Walsworth & M. D. Lukin, Storage of Light in Atomic Vapor, *Phys. Rev. Lett.* **86**, 783-786 (2001).
- [20] D. N. Matsukevich, & A. Kuzmich, Quantum State Transfer Between Matter and Light, *Science* **306**, 663 (2004).
- [21] L.-M. Duan, M. D. Lukin, J. I. Cirac & P. Zoller, Long-distance quantum communication with atomic ensembles and linear optics, *Nature* **414** 413-418 (2001).
- [22] Jones-Smith, K. & Mathur, H. Non-Hermitian quantum Hamiltonians with PT symmetry. *Phys. Rev. A* **82**, 042101 (2010).
- [23] El-Ganainy, R. *et al.* Non-Hermitian physics and PT symmetry. *Nat. Phys.* **14**, 11-19 (2018).
- [24] Hudelist, F. Kong, J. Liu, C. Jing, J. Ou, Z. Y. and Zhang, W. Quantum metrology with parametric amplifier-based photon correlation interferometers. *Nat. Commun.* **5**, 3049 (2014).
- [25] Du, S., ZHANG, S., ZHOU, S., YIN, G. Y. & BELTHANGADY, C. Two-dimensional magneto-optical trap for neutral atoms. *Patent* (2013).
- [26] Zhang, J., Gu, Z. J., Qian, P., Han, Z. G. & Chen, J. F. Cold Atom Cloud with High Optical Depth Measured with Large Duty Cycle. *Chinese Phys. Lett.* **32**, 064211

(2015).

- [27] Zeilinger, A. General properties of lossless beam splitters in an interferometry. *American J. Phys.* **49**, 882 (1981).
- [28] Hsiao, Y.-F. *et al.* Highly Efficient Coherent Optical Memory Based on Electromagnetically Induced Transparency. *Phys. Rev. Lett.* **120**, 183602 (2018).
- [29] Zhu, X., Wen, R. & Chen, J. F. Tunable atom-light beam splitter using electromagnetically induced transparency. *Phys. Rev. A* **97**, 063801 (2018).
- [30] Hammerer, K., Sørensen, A. S., & Polzik, E. S. Quantum interface between light and atomic ensembles. *Rev. Mod. Phys.* **82**, 1041-1093 (2010).
- [31] Lucamarini, M., Yuan, Z. L., Dynes, J. F. & Shields, A. J. Overcoming the fundamental rate-distance barrier of quantum key distribution without using quantum repeaters. *Nature* 1-6 (2018).

Methods

A cigar-shaped laser cooled ^{85}Rb atoms cloud is prepared in a two-dimensional (2D) magneto-optical trap (MOT) with a length of 1.5 cm, the temperature of the MOT is about $100\ \mu\text{K}$. The cooling laser is red-detuned from the transition $5S_{1/2}, F = 3 \leftrightarrow 5P_{3/2}, F = 4$ by 18 MHz with power as 110 mw. The repump laser is on resonance with the transition $5S_{1/2}, F = 2 \leftrightarrow 5P_{3/2}, F = 2$ which pumping the atoms to the cooling cycle. The experiment periodically time is 5 ms which 4.5 ms as MOT preparation time and 0.5 ms as measurement time

window. We use three-level EIT system to perform the MPBS. The probe and coupling laser, originated from the same diode laser, are respectively frequency shifted using acousto-optics modulators. The control laser (control, 795 nm) is blue detuned from the transition $|2\rangle = 5S_{1/2}, F = 3 \leftrightarrow |3\rangle = 5P_{1/2}, F = 3$ by Δ and two-photon resonant with probe light (probe, 795 nm) which is blue detuned from the $|1\rangle = 5S_{1/2}, F = 2 \leftrightarrow |3\rangle = 5P_{1/2}, F = 3$. They have same polarization σ^+ (or σ^-). The coupling beams is collimated with a diameter of 1.6 mm which can make the coupling beam recover whole cold atom cloud. The angle between the coupling beam and the atom long axis direction is 2.5° . A probe pulse (50ns) which created by the acousto-optic modulator (AOM) through radio-frequency (RF) signal splitting into two well separated pulses through a half wave plate, PBS, 20m polarization-maintained single-mode fiber and fiber BS, then they are launched into MOT and focused on the center of the cold atom cloud with diameter of $230\mu\text{m}$, the relative intensities of the two pulses can be modulated by half-wave plate aimed to make power match of the optical and the spin wave. The final optical signal collected by a photomultiplier tube (PMT). The first coupling pulse width is 120ns, the second coupling pulse width and the power are adjusted according to detuning and the OD to modulation atomic beams plitter ratio, the third is extended to 600 ns with maximum intensity to make sure collective atomic mode almost retrieved, the intensities of the three coupling pulse are controlled by an EOM. The single photon detuning Δ controlled by AOM and the OD through adjust the repump laser power.

The experimental procedure of the MPBS is shown in Fig 2(c), the two probe pulses (grey and pale green shadows) are generated by a single 50 ns duration pulse (300 nW) that split by an optical beam splitter, with a delay time of about 100 ns (20 m polarization-maintained single-mode fiber delay). Then, a long control pulse with 600 ns (faint yellow shadows in Fig 2(c)) is applied to the atom ensemble after the interference step, for both magnon readout and system initialization. Figures 2(c)-(e) show the outputs of the MPBS for the case of single photon detuning 30 MHz with an optical depth (OD) of 30. In the following experiments, we adjusted the coupling pulse intensities for the magnon preparation and interference steps to match the amplitudes of output photon and magnon. Figure 2(d) shows the results for single port input to MPBS (either photon or magnon be vacuum state), which shows that the outputs at two ports matches. Typical results for magnon-photon interference for different phase ϕ are shown in Fig. 2(e), which demonstrate the change of the outputs at different ports according to the interference. Here, since our real experimental time (about $1\mu\text{s}$) is very short compared with the cycling time (5 ms) and the phase uncertainty of the fiber is negligible [according to [31], phase drift during sin-

gle experiment cycle $< 18\text{ rad/ms}/200\text{km} \times 20\text{ m} \times 1\mu\text{s} \sim 1.8 \times 10^{-6}\text{ rad}$], the relative phase of the probe pulses is not controlled manually but fluctuate randomly. Therefore, we record the output intensities of photon and magnon in the phase diagram, where the intensity are obtained by integrating the areas of the output pulses (grey region and the rosiness region) in the Fig. 2(e).

Acknowledgments

This work is supported by the National Key Research and Development Program of China under Grant number 2016YFA0302001, and the National Natural Science Foundation of China through Grant No. 11674100, 11654005, 11234003, the Natural Science Foundation of Shanghai No. 16ZR1448200, and Shanghai Rising-Star Program 17QA1401300.